Li, H.; Thompson, D.; Squicciarini, G.; Liu, X.; Rissmann, M.; Denia, FD.; Giner Navarro, J. (2020). Using a 2.5D boundary element model to predict the sound distribution on train external surfaces due to rolling noise. Journal of Sound and Vibration. 486:1-22. https://doi.org/10.1016/j.jsv.2020.115599

Using a 2.5D boundary element model to predict the sound distribution on train external surfaces due to rolling noise

Hui Li[1*], David Thompson[1], Giacomo Squicciarini[1], Xiaowan Liu[1], Martin Rissmann[2], Francisco D. Denia[3], Juan Giner-Navarro[3]

[1]Institute of Sound and Vibration Research, University of Southampton, Southampton SO17 1BJ, United Kingdom
[2]Vibratec, Chemin du Petit Bois BP 36, F-69131 Ecully Cedex, France
[3]Centro de Investigación en Ingeniería Mecánica, Universitat Politècnica de València, Camino de Vera s/n, 46022 Valencia, Spain

Abstract

In order to be able to predict train interior noise, it is first important to calculate the external sound pressure distribution on the floor, sidewalls and roof. This can then be combined with the transmission loss of the train panels to determine the interior noise. Traditional techniques such as the finite element and boundary element (FE/BE) methods in three dimensions (3D) can achieve this result but are computationally very expensive. In this paper, a wavenumber-domain boundary element (2.5D BE) approach is instead adopted to predict the propagation of rolling noise from the wheels, rails and sleepers to the train external surfaces. In the 2.5D models, only the cross-section of the vehicle is represented by using boundary elements, while the third direction is considered in terms of a spectrum of wavenumbers. The rail is treated directly in the wavenumber domain but, to include the wheel, a method of representing point sources in a 2.5D approach is developed. An inverse Fourier transform is applied to obtain the spatial distribution of the sound pressure on the train surfaces. The validity of this approach has been verified by comparison with experimental data. The 2.5D BE method was first used to predict the sound distribution on a 1:5 scale train surfaces due to a point source below the vehicle, and later it was used to predict the sound pressure on a full-scale metro vehicle due to a loudspeaker. Comparisons of predictions with measurements on the scale model and on the metro vehicle showed good agreements. For a point source below the vehicle, the sound pressure levels on the train floor were found to be around 20 dB higher than on the sides, and the sound pressure on the train roof was negligible. The 2.5D BE method was also used to predict the sound pressure on the metro vehicle surfaces in running operation, in which the predicted sound pressure levels on the train external surfaces agreed with measurements to within 3 dB and similar trends were found in terms of spectra and longitudinal distribution of pressure.

Key words: 2.5D method, boundary element model, train external surfaces, rolling noise

1 Introduction

In developing new trains, one of the aspects to consider is the interior noise. With increasing train speeds and passenger demands, researchers and manufacturers are developing strategies to predict and mitigate noise transmission into the vehicles. Different approaches suitable for train interior noise prediction have been studied and adopted with different degrees of success. These include statistical energy analysis (SEA) [1, 2], a finite element (FE) method or hybrid FE-SEA approach [3, 4] and the ray-tracing method [5, 6]. All these methods require a good description of the noise sources, an estimate of the sound pressure distribution around the vehicle and a prediction of noise transmission through train wall structures. The aim of this paper is to present an approach capable of determining the exterior sound pressure distribution on the train walls due to rolling noise sources.

Among the various sources that radiate noise when a train travels along a track, rolling noise is often the dominant one. It is radiated by the vibration of the wheels, rails and sleepers, and propagates to the external surfaces of the train body. Rolling noise, including the interaction between the wheel and the track, has been well studied in recent decades and validated models exist, notably TWINS [7]. More recent research on railway rolling noise has led to improved models for the rail radiation [8, 9]. Besides, Zhang. et al. [10] proposed a model of a discretely supported track based on the waveguide finite element (2.5D FE) approach in order to improve the predictions of the vibration of the track. Very good agreement was found between their predictions and the measurement results, especially for the track with soft rail pads. Of interest is also the effect of slab tracks [11, 12] and the influence of the rail fastener stiffness [13].

Various strategies have been presented for determining the noise transmission through train wall structures, such as the SEA method and the 2.5D FE/BE approach. The SEA method can give understanding of how the energy flows through the complex wall structure of a train with high computational efficiency, which is beneficial at the early design stage. The 2.5D FE/BE approach is more accurate and gives a deeper understanding of the mechanism of noise transmission through complex walls. Both approaches can be used for both the airborne and the structure-borne paths. An example of the use of the SEA method to model the noise transmission through extruded panels was presented by Geissler and Neumann [14]; Xie et al. [15] also used the SEA method to predict the vibro-acoustic behaviour of aluminium extrusions.

Orrenius et al. [16] modelled the acoustic transmission through extruded profiles of railway vehicles by using SEA combined with the 2.5D FE method. Nilsson et al. [17] investigated the noise transmission through extruded panels using a coupled 2.5D FE/BE method. During recent years, new strategies for predicting the noise transmission through extruded walls with the influence of mean flow on the outer surface [18] and including porous materials [19] have also been developed. All these have increased the understanding of how sound is transmitted through complicated extruded structures that are commonly used in trains or aeroplanes. However, in addition to the sound transmission properties of the walls enclosing the interior of a vehicle, it is necessary to know the distribution of sound pressure on the exterior surfaces of the vehicle to be able to predict the interior noise.

Zheng et al. [20] presented a comprehensive model for the interior noise of a high-speed train, in which all the main exterior noise sources were considered. The strength of the noise sources and the transmission from the sources to the train walls were obtained mainly from measurements or from simulations using commercial software based on boundary element analysis or computational fluid dynamics; however, the details of the modelling strategies of the sources were not given in detail. Bistagnino et al. [6] compared a Fast Multipole BEM and beam-tracing technique with measurements of the sound pressure on the train walls due to loudspeakers placed close to the wheels. The predictions from both methods agreed well with the measurements, but the need to deal with complicated train structures in 3D domain makes the procedure difficult to handle at a design stage. Kohrs et al. [21] compared different approaches and methods, including BEM, ray tracing and SEA to calculate the pressure field around the car body for either artificial sources or real operation in free field and in tunnel. Acceptable accuracy was achieved although various simplifications and assumptions had to be made and there were uncertainties in the various parameters involved.

In this paper, the 2.5D BE method is introduced with the aim of predicting the sound pressure on the train external surfaces due to rolling noise. One of the first applications of the 2.5D BE method was made by Duhamel [22] to predict the sound pressure around a noise barrier and the method showed a high efficiency to solve such 3D acoustic problems with effectively 2D geometry. In the current work, the wheels, the rails and the sleepers are represented as noise sources in a 2.5D model that accounts for the train cross-section and includes the presence of the ground. The rail is treated directly in the wavenumber domain but, to include the wheel, a method of representing point sources in a 2.5D approach is developed. The numerical approach

is briefly described in Section 2 and methods to include fundamental sources into the 2.5D domain are introduced, while Section 3 explains how the rolling noise sources are represented in the 2.5D model. Experimental validation is presented based on both laboratory and field measurements. Section 4 verifies the validity of this approach by means of comparisons with laboratory tests on a scale model in an anechoic chamber. Section 5 presents comparisons with field measurements of the sound pressure on the sidewalls of a train.

2 Numerical model

2.1 2.5D boundary element method

The derivation of the 2.5D BE method starts from a 3D problem. Assuming time-harmonic variations with dependence $e^{i\omega t}$, the boundary integral for a 3D acoustic problem is [23]

$$p(x',y',z') = -\int_S \Big(i\rho\omega v(x,y,z)\psi(x,y,z|x',y',z') + p(x,y,z)\frac{\partial\psi(x,y,z|x',y',z')}{\partial n}\Big) dS \tag{1}$$

where S is the surface of the boundaries that represent the problem, $p(x',y',z')$ is the sound pressure amplitude at a receiver P, ρ is the density of air, $v(x,y,z)$ and $p(x,y,z)$ are the normal velocity and pressure amplitudes on the surface and $\psi(x,y,z|x',y',z')$ is the Green's function, i is the imaginary part and ω is the angular frequency. If the geometry of the problem can be considered uniform and of infinite length in one direction, e.g. x, Equation (1) can be conveniently solved in the 2D domain for a range of wavenumbers k_x in the x direction. To achieve this, the Fourier transform pair for the sound pressure $p(x,y,z)$ with respect to x is introduced

$$\tilde{p}(k_x,y,z) = \int_{-\infty}^{\infty} p(x,y,z)\, e^{ik_x x} dx \tag{2}$$

$$p(x,y,z) = \frac{1}{2\pi}\int_{-\infty}^{\infty} \tilde{p}(k_x,y,z)\, e^{-ik_x x} dk_x \tag{3}$$

The spatial distribution of sound pressure can then be obtained from Equation (3) once $\tilde{p}(k_x, y, z)$ is determined. This can be achieved through a 2.5D formulation of Equation (1) in which the pressure, velocity and Green's function are expressed as functions of k_x, y and z and the boundary integrals are solved over the perimeter of the boundary region Γ in the *y*-*z* plane. The wavenumber domain integral equation therefore becomes:

$$\tilde{p}(k_x, y', z') = -\int_{\Gamma} \Big(\mathrm{i}\rho\omega\tilde{v}(k_x, y, z)\psi(k_x, y, z|y', z') + \tilde{p}(k_x, y, z)\frac{\partial\psi(k_x, y, z|y', z')}{\partial n} \Big) \mathrm{d}\Gamma \tag{4}$$

$\tilde{v}(k_x, y, z)$ in Equation (4) is the velocity normal to the surface in the wavenumber domain, which is given by the Fourier transform of the normal velocity in the spatial domain, similar to Equation (2). In Equation (4), the wavenumber in the *x* direction, k_x, is independent of *y* and *z* and the Green's function $\psi(k_x, y, z|y', z')$ takes the same form as the 2D fundamental solution [22]

$$\psi(k_x, y, z|y', z') = -\mathrm{i}\frac{1}{4}H_0^{(2)}((k_0^2 - k_x^2)^{1/2}r) \tag{5}$$

with $H_0^{(2)}(x)$ being the Hankel function of the second kind and zero order, and k_0 the wavenumber in air. If $k_x > k_0$, the wavenumber in the 2D domain is imaginary, and the sound waves will decay exponentially with distance $r = (y^2 - z^2)^{1/2}$.

2.2 Ground effect

The presence of a rigid ground can be considered by means of an image source located symmetrically beneath the ground. If a rigid ground is considered, the modified Green's function takes the form [22]

$$G = -\frac{\mathrm{i}}{4}H_0^{(2)}((k_0^2 - k_x^2)^{1/2}r) - \frac{\mathrm{i}}{4}H_0^{(2)}((k_0^2 - k_x^2)^{1/2}r') \tag{6}$$

where *r* is the distance from the actual source to the receiver, and r' is the distance from the image source to the receiver. The phase difference between the contributions of these two sources is included automatically in this equation.

Partially absorbing boundaries can be modelled through their surface normal impedance, which can be obtained by means of analytical or empirical models. In this case the corresponding part of the boundary is meshed using boundary elements. For simplicity the Delany-Bazley [24] model for the impedance is adopted in the current work to model the sound reflection from a partially absorbing surface.

2.3 Fundamental sources in 2.5D

For use in a railway noise study, this method needs to handle discrete compact sources, such as monopoles and dipoles, as well as extended sources, such as the rail. One of the challenges is to represent discrete sources in a 2.5D model, where by definition the different components of the model extend indefinitely in the x direction. This is achieved by applying suitable wavenumber spectra to equivalent extended sources.

2.3.1 Monopole source

In 3D, a monopole source can be represented as a pulsating sphere, but this is not possible in a 2.5D domain approach. To approximate a monopole, a circle is meshed in the *y*-*z* plane. The boundaries of the circle are assigned a unit normal velocity and a spatial window is applied in the x direction with its shape set through its wavenumber spectrum. The distribution of the velocity is chosen to be constant in the x direction over a length corresponding to twice the radius of the circle a, such that:

$$v_n(x) = \begin{cases} 1 & x \in [-a, a] \\ 0 & x \notin [-a, a] \end{cases} \tag{7}$$

The corresponding velocity in the wavenumber domain is given by

$$\tilde{v}_n(k_x) = 2\frac{\sin(k_x a)}{k_x} \tag{8}$$

The velocity distribution in the *x* direction and in the wavenumber domain are plotted in Figure 1(a) and (b) respectively. Thus, the source in the 2.5D model corresponds to a pulsating cylinder of radius a and length $2a$. This has the same volume velocity as a pulsating sphere of radius a. Additionally, however, as the geometry of the source extends indefinitely in the x direction, the numerical model contains a cylinder that is rigid for $|x| > a$.

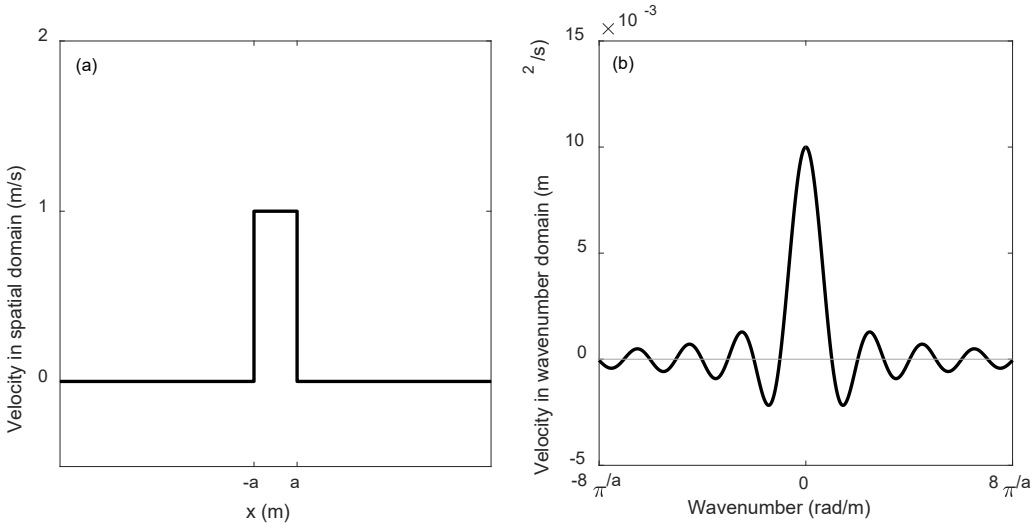

Figure 1. (a) Velocity distribution of the monopole source in the x direction and (b) its wavenumber spectrum.

To verify the validity of this representation of the source, a circular source was represented in the 2.5D model by 36 linear boundary elements. The sound pressure levels around the monopole-like source calculated by using the 2.5D model were compared with the theoretical results for a pulsating sphere [25]. In the 2.5D model, the volume velocity was fixed as 10^{-5} m^3/s and the source radius was varied from 0.001 m to 0.1 m. The frequency varies from 100 Hz to 5 kHz. The comparisons were made in terms of the sound pressure levels at receivers on a circle 5 m away from the source centre, in both the x-y and y-z planes. The definition of the two planes is illustrated in Figure 2. A total of 72 receivers is considered in each plane, with a separation of 5°, but omitting the points on the x axis.

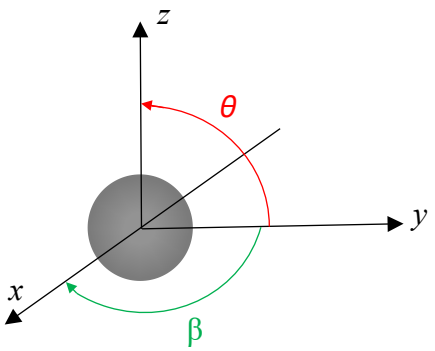

Figure 2. The definition of the coordinates for the source.

The maximum errors between the 2.5D predictions and the analytical solutions are plotted against the product of the acoustic wavenumber and the radius of the source in Figure 3.

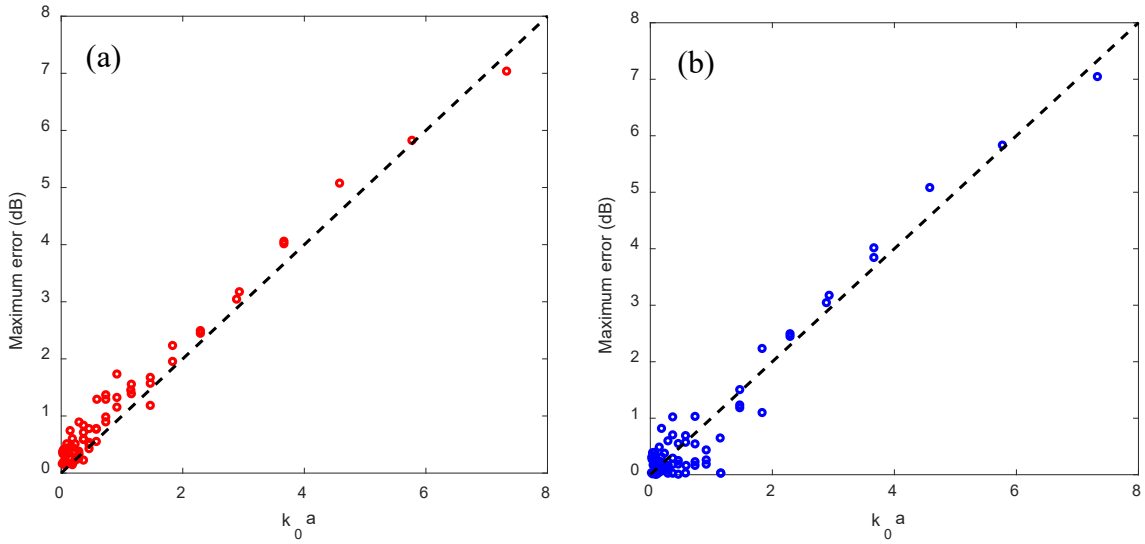

Figure 3. (a) Errors for receivers in the *x*-*y* plane, (b) errors for receivers in the *y*-*z* plane.

It is found from Figure 3 that the difference between the predictions and the analytical solutions increases with increasing k_0a. Therefore, by making a small, its influence can be minimised. Provided that k_0a is smaller than 0.5, the errors are less than 1 dB. Figure 4 gives an example of the sound pressure levels obtained from the 2.5D model compared with the analytical solutions at 5000 Hz for a source radius of 0.005 m (giving k_0a = 0.45). In the *y*-*z* plane, the 2.5D prediction and the analytical solution are within 0.4 dB of each other. In the *x*-*y* plane, the prediction has some fluctuations at around 90° and 270°, where the receivers are close to the cylinder, but the maximum error is less than 0.9 dB. These comparisons demonstrate that the 2.5D model proposed for a monopole source can be used reliably.

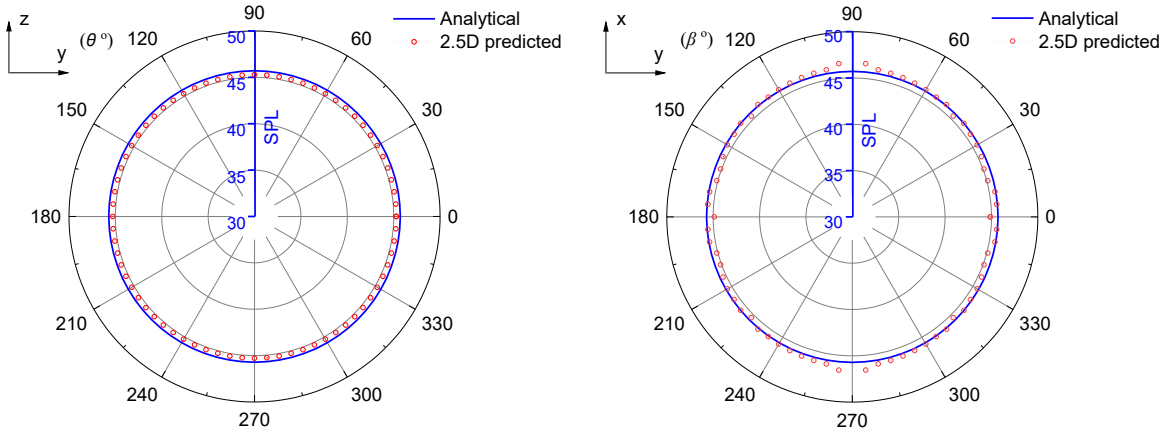

(a) (b)

Figure 4. Sound pressure level distribution (in dB) around a pulsating sphere with volume velocity 10^{-5} m^3/s and corresponding 2.5D model, radius 0.005 m, at 5000 Hz. The receivers are on a circle 5 m away from the source centre. (a) In *y*-*z* plane; (b) in *x*-*y* plane.

2.3.2 Dipole source

In a similar way, a dipole source in 3D can be represented by an oscillating sphere. In the 2.5D model, this velocity pattern is applied to the same circular grid: the normal velocity in the *y*-*z* plane is expressed as $v_n(y,z) = v\cos\theta$, where θ is the angle relative to the direction of oscillation, that is the *y* direction, see also Figure 2. The velocity distribution in the *x*-direction is given by

$$v_n(x) = \begin{cases} v\cos\left(\dfrac{2\pi}{4a}x\right) & x \in [-a,a] \\ 0 & x \notin [-a,a] \end{cases} \tag{9}$$

and the corresponding velocity in the wavenumber domain is given by

$$\tilde{v}_n(k_x) = v\left[\frac{\sin\left[\left(k_x+\frac{\pi}{2a}\right)a\right]}{k_x+\frac{\pi}{2a}} + \frac{\sin\left[\left(k_x-\frac{\pi}{2a}\right)a\right]}{k_x-\frac{\pi}{2a}}\right] \tag{10}$$

The representation of the velocity in the spatial domain and in the wavenumber domain is shown in Figure 5(a) and (b) respectively.

Similar to the monopole source, the 2.5D model represents approximately an oscillating cylinder of radius a and length $2a$ for the dipole source. As the geometry of the source extends indefinitely in the x direction, the numerical model again contains a cylinder that is rigid for $|x| > a$.

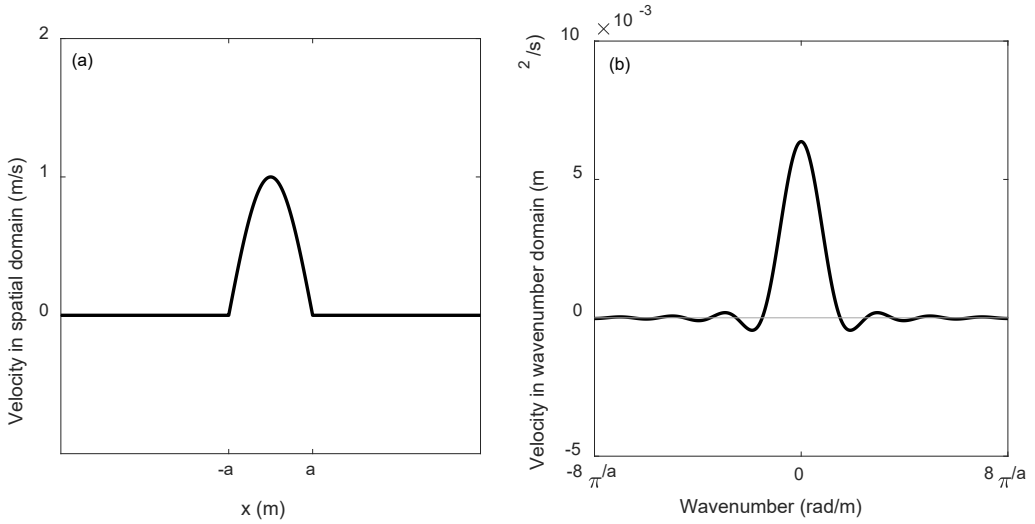

Figure 5. (a) Velocity distribution of the dipole source in the *x* direction and (b) its wavenumber spectrum.

As the source strength of a dipole depends on the distance between the positive and negative parts of the source as well as their individual strengths, its size should be taken into account in determining the source strength to be used in the 2.5D model that corresponds to a particular dipole. Assuming that the amplitude of the oscillating velocity of the surface is **V**, the dipole source strength of the oscillating sphere (or of the 2.5D model) can be calculated by

$$Q = \int_S (\mathbf{V} \cdot \mathbf{d}) \mathrm{d}S \tag{11}$$

where **d** is the distance vector to the surface from its centre and S is the surface area. The dipole source strength of an oscillating sphere of radius a is $\pi a^3 V$ (where V is the magnitude of the oscillating velocity) and that of the 2.5D model is $4a^3V$. Thus, for an oscillating sphere and the corresponding 2.5D model of the same radius, a factor of $\pi/4$ is required between their velocities.

To check the validity of the 2.5D model, it has been used to predict the sound distribution around an oscillating source with different radii and at a number of frequencies. It is found that

the maximum error between the 2.5D predictions and the analytical solutions increases with the product of the acoustic wavenumber and the source radius, similar to what has been found for the monopole case. Figure 6 gives an example of the sound pressure levels obtained from the 2.5D model compared with the analytical solutions at 5000 Hz for an oscillating sphere with radius 0.005 m (36 linear elements were again used to represent the source in the 2.5D model). This shows the sound distribution at the receivers on a circle of radius 5 m around the dipole which has an oscillating velocity amplitude of 1 m/s. The numerically predicted sound distribution in the *y*-*z* plane is almost identical to the analytical values (within 0.1 dB). As expected, there are some fluctuations in the *x*-*y* plane when β is approaching 90° and 270°, which is about 1.3 dB in this case (seen from Figure 6(b)), but as the sound pressure levels at these angle regions are small, they will not significantly affect the validity of the 2.5D model.

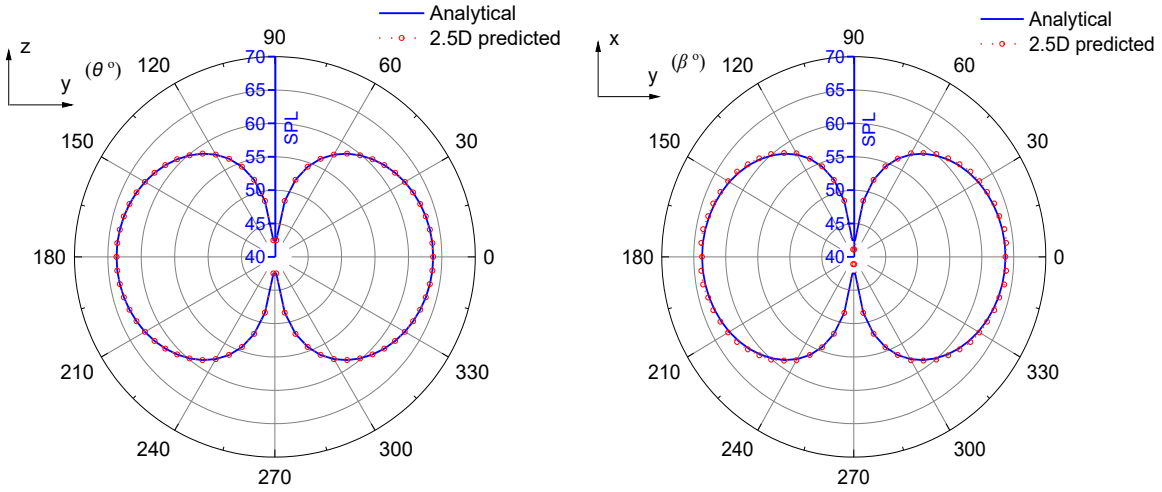

(a) (b)

Figure 6. Sound pressure level distribution (in dB) around an oscillating sphere and corresponding 2.5D model, oscillating velocity amplitude 1 m/s, radius 0.005 m, at 5000 Hz. (a) In *y*-*z* plane; (b) in *x*-*y* plane.

3 Rolling noise

3.1 Wheel noise

The sound radiation from a train wheel can be divided into two components: axial and radial [26]. The sound directivity of the radial component can be represented approximately as a monopole while that of the axial component can be approximated as a horizontal dipole. In the 2.5D model, the radial component is modelled by implementing a monopole-like source and

the axial component is modelled by a dipole source using the formulation described in the previous section. In the boundary element calculations, the velocities of the sources are set to unity and the final results are re-scaled to correspond to the sound power levels calculated in TWINS.

A wheel with diameter of 0.86 m is studied, and it is represented in the 2.5D model by using a point source located at its geometrical centre. This has been compared with a model in which three point sources at different heights were used to represent the wheel, but it is found that the sound pressure spectra at the receivers on the train side surfaces above the bogie obtained from the two models are similar. The difference in terms of overall sound pressure levels at those receivers was less than 0.5 dB. Therefore, only a single point source is used in this work to reduce the computational cost.

3.2 Rail noise

The rail is an extended source in the longitudinal direction which can be represented directly by its vibrating surface using the 2.5D BE method. The coordinate system of the rail as well as its vertical and lateral vibration are illustrated in Figure 7. The vertical vibration of the rail is defined in the x-z plane and the lateral vibration is defined in the x-y plane. The structural wavenumber k_x is introduced by applying the Fourier transform to the mobility of the rail. k_0 is the acoustic wavenumber, as defined before. In Figure 7, the wavenumber arrows only illustrate the relation between the structural wavenumbers and the acoustic wavenumber, because in fact both the vertical and lateral vibration of the rail can radiate sound to the whole spatial domain. The noise radiation from the vertical and lateral vibration of the rail are considered separately.

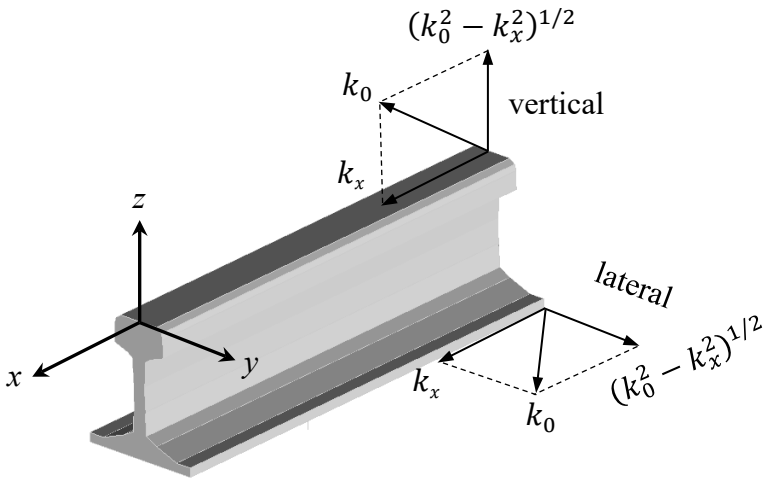

Figure 7. The definition of the coordinates of the rail and the vibration direction.

The response of the rail to a unit force is calculated in terms of its transfer mobility $Y(x)$ at a distance x from the excitation point and circular frequency ω from a model of a Timoshenko beam on a continuous two-layer foundation [27] in which the sleepers are represented by an equivalent continuous layer of mass. This can be expressed as

$$Y(x) = u_1 \mathrm{e}^{-\mathrm{i}k_r|x|} - \mathrm{i}u_2 \mathrm{e}^{-\beta|x|} \tag{12}$$

where k_r is the structural wavenumber corresponding to the predominantly propagating wave, β is the one corresponding to the evanescent wave and u_1 and u_2 are the corresponding wave amplitudes; these wavenumbers and amplitudes include the effect of the support layers [26]. The vertical and lateral mobilities of the rail are obtained using the same model. The results are calculated with the data shown in Table 1, which correspond to a 54E1 rail in a track with concrete sleepers used for validation in Section 5 below; the sleeper spacing of 1 m present at the test site is untypically large.

Table 1. Parameters used to represent a railway track.

	Vertical	Lateral
Rail bending stiffness (Nm^2)	4.86×10^6	0.88×10^6
Rail shear coefficient	0.4	0.4
Rail loss factor	0.02	0.02
Rail mass per length (kg/m)	54	
Cross receptance level (dB)	-7	
Pad stiffness (N/m)	800×10^6	100×10^6

Pad loss factor	0.2	0.2
Sleeper mass (half, kg)	150	
Distance between sleepers (m)	1.0	
Ballast stiffness (N/m)	100×10^6	35×10^6
Ballast loss factor	1.0	2.0

The real part of k_r corresponds to the wavenumber of the propagating waves along the rail and is plotted in Figure 8(a). The acoustic wavenumber in air is shown for comparison. The imaginary part of k_r corresponds to the decay with distance along the rail, which can be expressed as a track decay rate (TDR) in dB/m [26] as $\Delta = -8.686\mathrm{Im}(k_r)$. The decay rates of the rail for vertical and lateral vibration, obtained using the parameters from Table 1, are plotted in Figure 8(b).

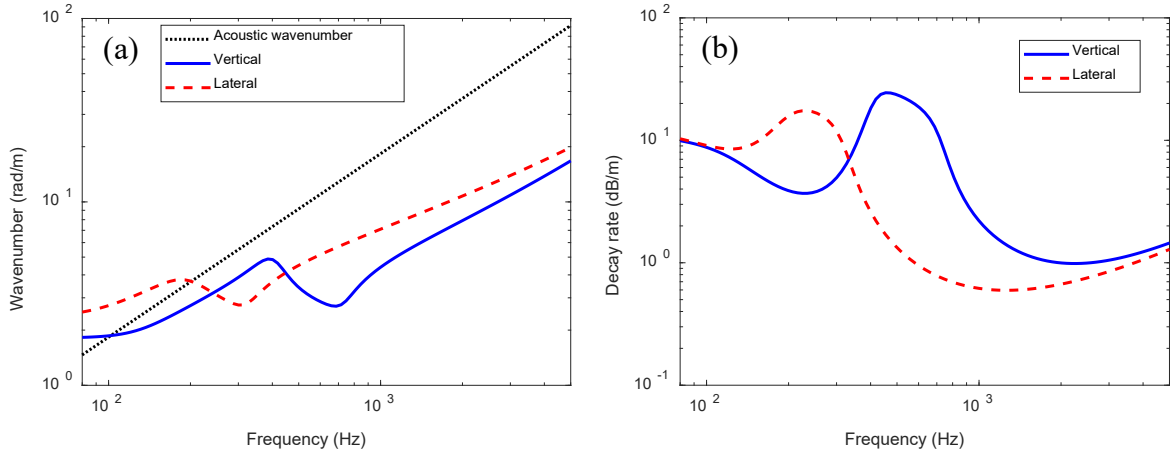

Figure 8. (a) Wavenumbers of the propagating waves, (b) calculated decay rates of the rail for vertical and lateral vibration.

The transfer mobility of the rail from Equation (12) is a function of *x* and its real and imaginary parts are illustrated for the vertical direction at two example frequencies in Figure 9. Figure 9(a) shows the results at 125 Hz, where the decay rate is relatively high and the wavelength is long, while Figure 9(b) shows the results at 2000 Hz with a relatively low decay rate and short wavelength.

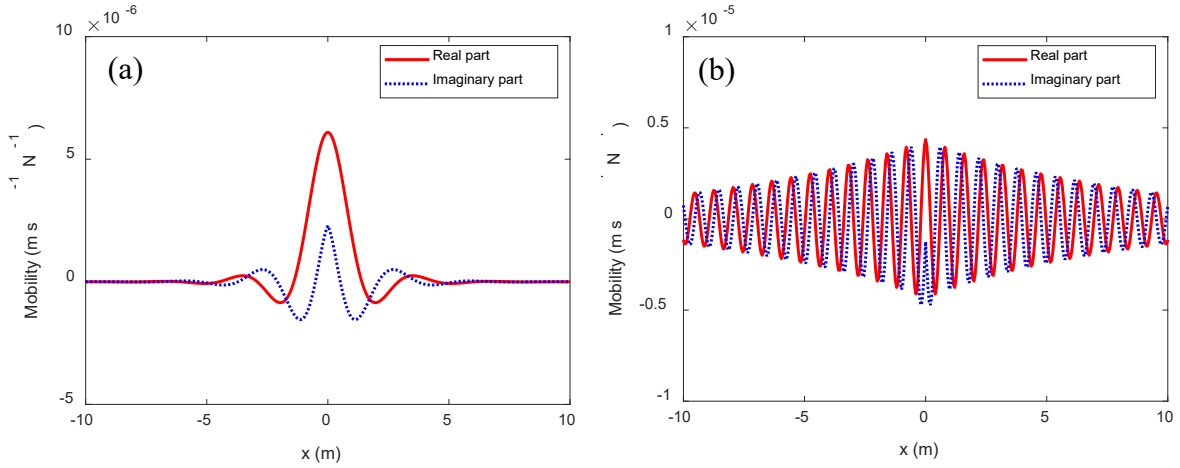

Figure 9. Rail transfer mobility for the vertical direction as a function of x in the spatial domain. (a) 125 Hz, (b) 2000 Hz.

Applying a Fourier transform to the transfer mobility in the spatial domain, the velocity in the wavenumber domain due to a unit force at $x = 0$ can be expressed as

$$\tilde{Y}(k_x) = u_1\left(\frac{1}{\mathrm{i}(k_r + k_x)} + \frac{1}{\mathrm{i}(k_r - k_x)}\right) - \mathrm{i}u_2\left(\frac{1}{\beta + \mathrm{i}k_x} + \frac{1}{\beta - \mathrm{i}k_x}\right) \tag{13}$$

where k_x is the wavenumber in the x direction introduced by the Fourier transform, which runs from -∞ to ∞. The mobilities in the wavenumber domain corresponding to Figure 9 are shown in Figure 10. At high enough frequency, once propagating waves have cut on in the rail, the wavenumber spectrum is dominated by the free wavenumber in the rail; at 2 kHz this can be seen as the peak at about 8 rad/m (see also Figure 8).

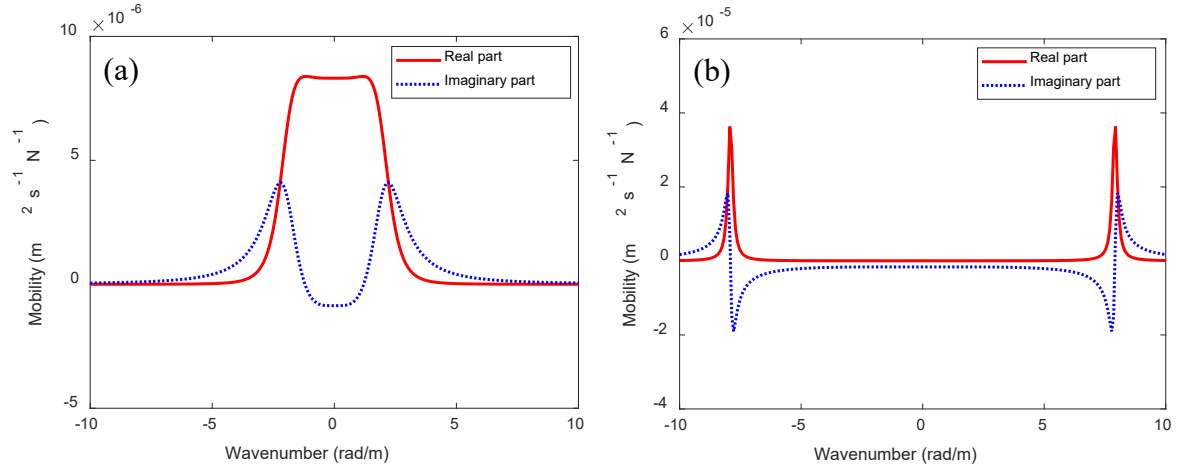

Figure 10. Rail mobility in the wavenumber domain. (a) 125 Hz, (b) 2000 Hz.

When k_x is smaller than the wavenumber in the air, the structural waves will produce propagating sound waves. In such a situation, the vibration of the rail radiates sound efficiently. However, when k_x is greater than the wavenumber in air, near-field sound waves will be generated (see Equation (5)) and these structural waves radiate sound inefficiently. However, the near-field sound waves cannot be neglected, especially at low frequency and in the region relatively close to the source. Neglecting them would introduce errors in the inverse Fourier transform when converting the sound pressure back to the spatial domain.

Finally, to obtain the radiation from the rail, the mobility in the wavenumber domain is applied as a velocity boundary condition to the boundary elements representing the rail cross-section. The rail cross-section is assumed to move uniformly in either vertical or lateral direction; the vibration in the vertical and lateral directions is dealt with separately. For simplicity, cross-section deformation of the rail [26] is not included in this study, although it could be included by using a 2.5D FE model of the rail instead of the Timoshenko beam model [8, 28].

3.3 Sleeper noise

The vibration of the sleepers is also required to determine their contribution to the noise in the 2.5D model. This vibration can be derived from the vertical rail mobility and from the ratio of the sleeper displacement to that of the rail. This is equal to [26]

$$r = \frac{s_p}{s_p + s_b - \omega^2 m_s} \tag{14}$$

where s_p is the complex rail pad stiffness in the vertical direction including damping, s_b is the complex ballast stiffness and m_s is the sleeper mass. An example result is shown in Figure 11 for the parameters shown in Table 1.

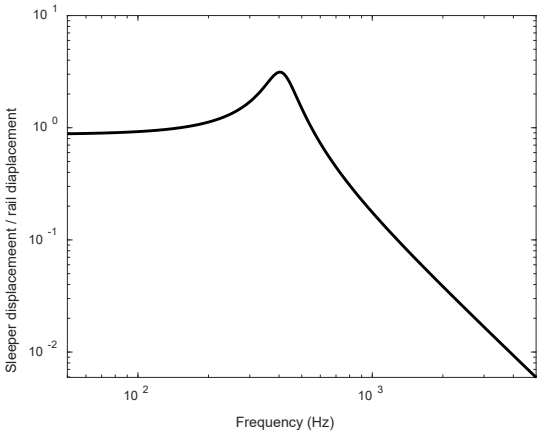

Figure 11. Ratio of sleeper displacement to that of the rail.

In ballasted track, the sleepers are embedded in ballast, so the vibrational velocity is only given to their top surfaces. Moreover, the 2.5D model treats the sleepers as a continuous medium in the x direction. To account for their discrete distribution and for the spacing between them, scaling factors are needed to adjust the sound power calculated from the 2.5D model. To calculate these scaling factors, a Rayleigh integral approach [29] was used to calculate the sound power of discrete sleepers. Different scaling factors were found to be necessary [30] for the low and high frequency regions in the 2.5D model to adjust the predictions and match the results obtained by using the Rayleigh integral. It was found [30] that, at high frequency where the acoustic wavelength is smaller than the sleeper spacing, the sound power needs to be adjusted by a factor corresponding to the ratio of the sleeper width to the sleeper spacing, here 1/5. At low frequency, where the wavelength is greater than the sleeper spacing, the scaling factor corresponds to the square of that ratio.

3.4 The 2.5D model

The wheels, the rails and the sleepers are considered as separate sources in the 2.5D model and the different components are combined incoherently to obtain the total pressure distribution over the train surfaces.

Figure 12(a) shows the cross-section of the 2.5D model used for investigation of the noise transmission from the wheel to the train external surfaces. The wheel contribution is modelled by using the monopole and dipole sources as outlined in Section 2.3. Figure 12(b) shows the cross-sections adopted to calculate the contribution of the rail, with the rail foot located 0.02 m above the ballast. The rail velocity is obtained in the wavenumber domain (Section 3.2) and is

assigned to the cross-section of the rail. In the 2.5D models for the wheel and the rail, the sleepers are omitted and the ballast is replaced by a rectangular box sitting on the ground with a height of 0.05 m. Its upper surface is modelled by means of its surface normal impedance based on the Delany-Bazley model with an equivalent flow resistivity of 50 kPa s/m^2 [31]. The cross-section adopted to calculate the contribution from the sleepers is shown in Figure 12(c). The velocity of the sleepers in the wavenumber domain is calculated as described in Section 3.3 and is assigned to their upper surface (the ballast is ignored). In these three numerical models, the modified Green's function in Equation (6) is used, which presents a half-space ground extending beyond the region modelled using boundary elements.

Linear boundary elements are used to create these models. 36 elements are used to model the fundamental sources representing the wheel in Figure 12(a), which are modelled by using a circle of radius 0.005 m. 100 elements are used to model the rail cross-section in Figure 12(b). The rectangular box used for the ballast in Figure 12(a) and (b) and for the sleepers in Figure 12(c), and the train body in all three models, are made of elements with size 0.02 m. As this is an exterior radiation problem, Five 'CHIEF' points are used inside the train and three are used in the rectangular box to overcome the non-uniqueness problem associated with resonances of the corresponding interior problem [32]. The train cross-section in Figure 12(a) does not include the side fairings whereas side fairings are present in Figures 12(b) and 12(c). Frequently, trains such as the one adopted in the validation tests described in Section 5 do not have fairings to cover the bogie area and the model approximates this by using different cross-sections for the models of the wheel and track components of noise.

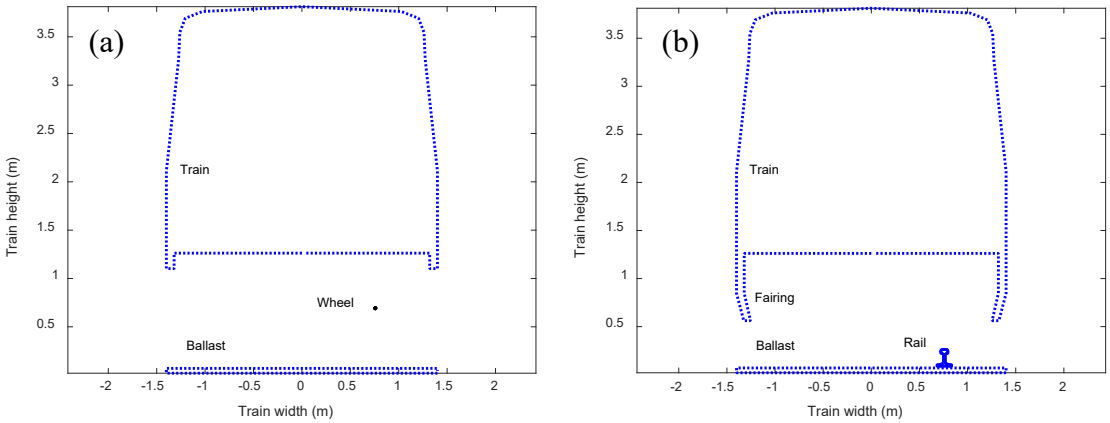

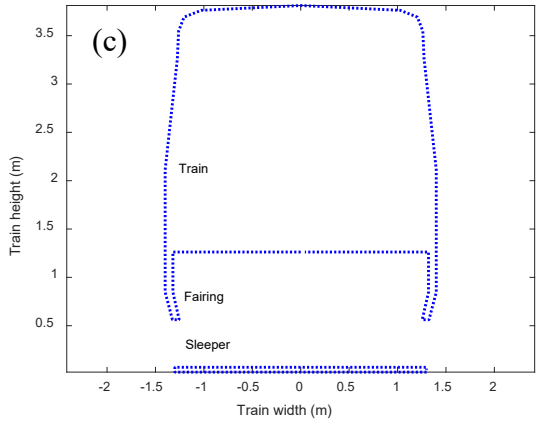

Figure 12. 2.5D models for (a) the wheel, (b) the rail, (c) the sleepers.

The 2.5D models give the sound pressure on the train cross-section in the wavenumber domain. After applying the inverse Fourier transform, the sound pressure distribution in the spatial domain is then obtained. The source strength in the 2.5D models for the wheel is based on a unit velocity and that for the rail is based on a unit force. The sound power of the wheel, the rail and the sleepers obtained from the TWINS model are used to re-scale the results from the 2.5D model. The total sound pressure on the train surfaces is then determined from the incoherent sum of the contributions of the wheel radial and axial components, the rail vertical and lateral components, and the sleeper component.

4 Experimental validation on scale models

To validate the modelling approach used to predict the sound distribution on the train external surfaces, results from two different sets of measurements have been used. In the first of these, laboratory measurements were performed in an anechoic chamber at the University of Southampton, which are presented in this section. A 1:5 scale train model is used [33], which is made from dense foam that has been varnished to minimise its absorption. In addition, a 1:5 scale track model [34] that is composed of steel rails, concrete sleepers and ballast was created. These were located in the anechoic chamber, as shown in Figure 13(a). The track is 2 m long and 0.8 m wide, and the train is 2.5 m long, 0.56 m wide and has a height of 0.45 m. The rail head is 0.036 m above the top of the sleepers and 0.19 m below the train floor. The model was located on a wooden ground plane (18 mm thick) that was 0.256 m below the rail head. With this arrangement, the sound pressure distribution around the scale model railway vehicle was determined using a point source and a vibrating rail.

4.1 Point source

To evaluate the sound pressure distribution around the train body due to a point source, a horn driver unit driven by white noise was connected to a tube with an orifice (diameter 15 mm), which gives a broadly non-directional output. The source strength was determined by a free-field measurement. It is assumed that its volume velocity is independent of the source location. The orifice of the source was then located beneath the train floor, directly above one of the rails and 0.32 m from one of its ends, see Figure 13(b). Microphones were located along the centrelines of the four external surfaces of the train: the floor, two walls and the roof. On each surface, there were 21 measurement locations with a spacing of 0.1 m; these sets of points are indicated as P_1, P_3, P_4, P_5 in the corresponding numerical model in Figure 14. Another set of microphones was placed along the upper right-hand corner on the side face, indicated as P_2.

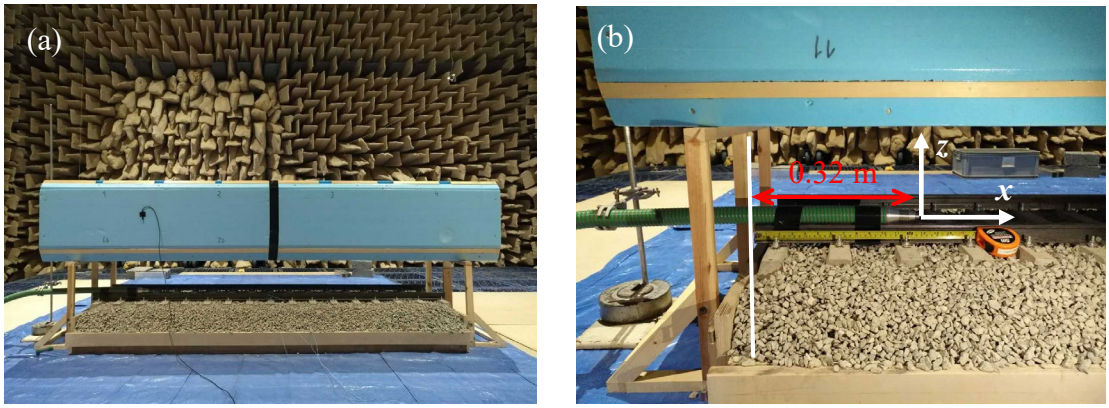

Figure 13. Measurement arrangement in laboratory test for point source. (a) Overview and (b) source location.

The receivers in the numerical model (Figure 14) were located at the same locations as those in the measurements. The source was represented in the 2.5D model by a monopole, as described in Section 2.3, with a radius of 0.005 m and a source strength corresponding to the one in the experiments. The ground was set to be rigid in the 2.5D model and the ballast and track bed were modelled by a rectangular box with an impedance boundary condition on its upper surface and with rigid condition on its sides.

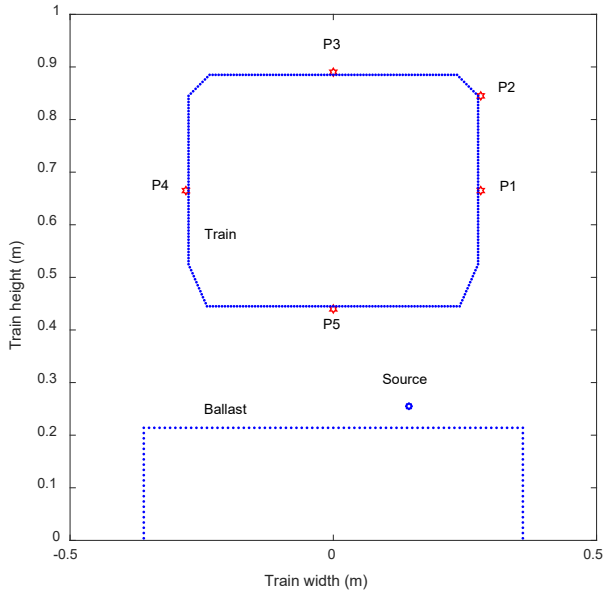

Figure 14. The 2.5D model used for predicting noise on train outside surfaces of the scale model due to a point source.

Figure 15 shows a comparison of the predicted sound levels with the measured ones at P_2 (the upper corner position) for four frequency bands. The distance x is shown relative to the location of the source. These results are shown for the 1000 Hz, 1600 Hz, 2500 Hz, and 4000 Hz one-third octave bands for the scale train model, which correspond to 200 Hz, 315 Hz, 500 Hz and 800 Hz at full scale. In the numerical models, results were calculated at three frequencies in each band and averaged to obtain the sound pressure level in the band.

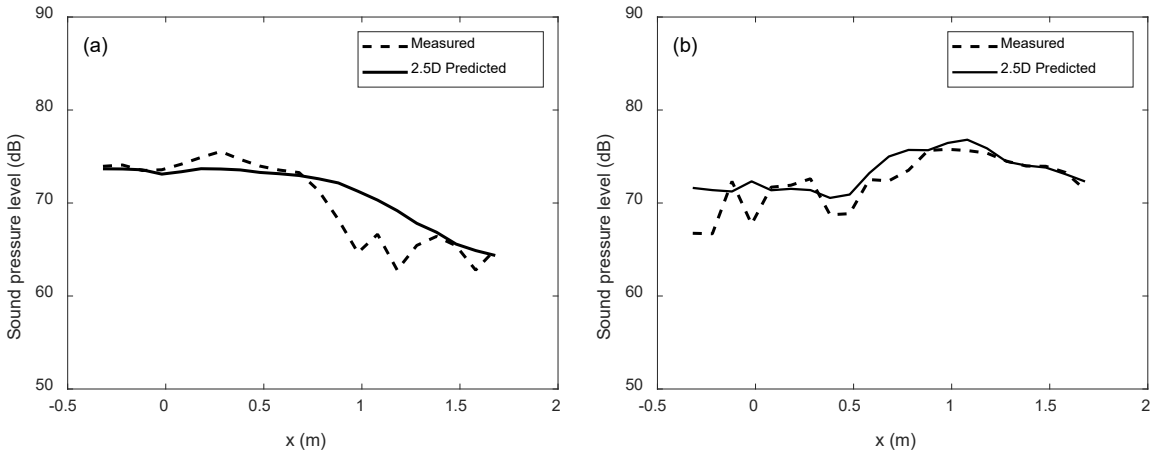

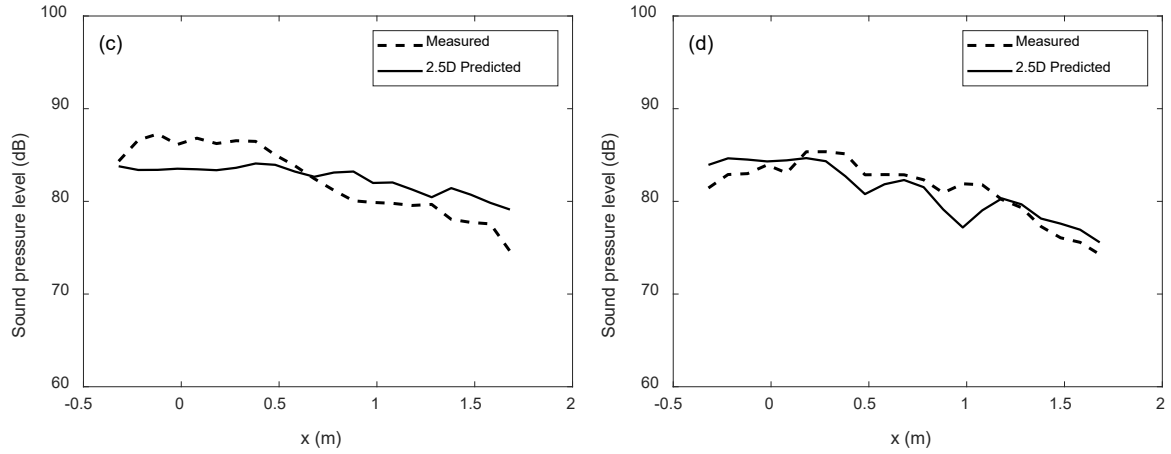

Figure 15. Sound pressure level comparison in four one-third octave bands at the right up corner point, dB re 2.0×10^{-5} Pa. The distance x is shown relative to the location of the source. (a) 1000 Hz, (b) 1600 Hz, (c) 2500 Hz, (d) 4000 Hz.

Figure 16 shows the equivalent results on the four different train surfaces. These results are given for the 4 kHz one-third octave band as an example; the results in the other one-third octave bands are similar.

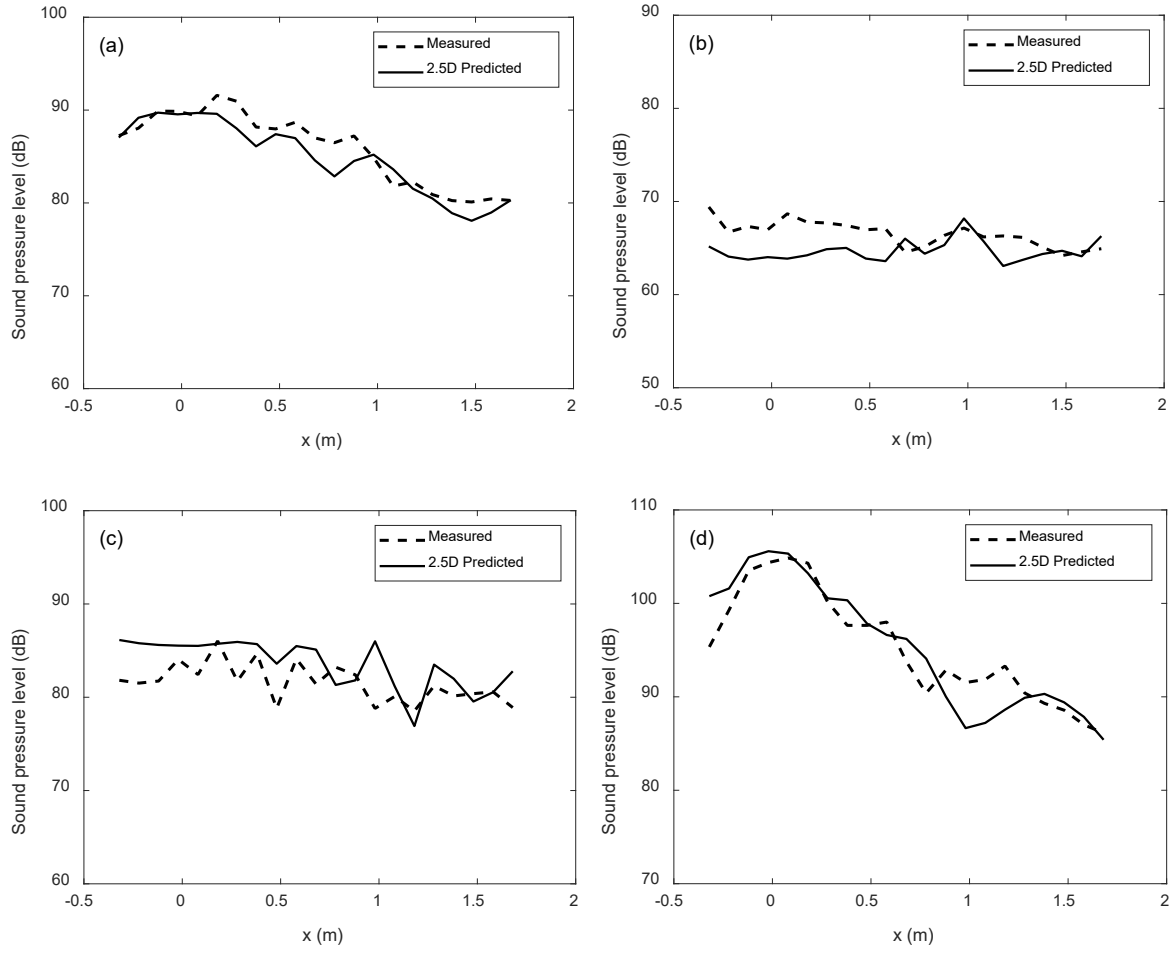

Figure 16. Sound pressure level comparison at the four surfaces in the 4 kHz one-third octave band, dB re 2.0×10^{-5} Pa. (a) On the right side, P_1, (b) on the top, P_3, (c) on the left side, P_4, (d) on the bottom, P_5.

From Figures 15 and 16, it can be concluded that the 2.5D BE approach is able to give reasonable predictions of the sound pressure levels on the train external surfaces due to a point source below it. The maximum errors at each measured position (predicted level minus measured level) and the average difference between the predictions and the measurements are listed in Table 2 for each frequency band. As the 2.5D model corresponds to an infinite carriage, the truncation at the end of the carriage may have some effect on the agreement but for measurement points close to the carriage wall the effect is expected to be small. When calculating the difference between the predictions and the measurements the two data points at each end are ignored. At the upper corner position P_2, the average difference between the prediction and the measurement is less than 3 dB in most of the 1/3 octave bands. The maximum difference at position P_2 is found in the 2000 Hz band and at the measurement positions located close to one of the ends of the carriage. The results in Figure 16 and Table 2 indicate that the 2.5D model gives better predictions of the sound pressure on the bottom (P_5) and the side surface that is closer to the source (P_1). Larger errors are found at the receivers on the top (P_3) and the side that is further from the source (P_4).

Table 2. Level differences between predictions and measurements for point source below the scale model train body (dB). Maximum (Max.) and average (Ave.) difference over 17 points at each location.

Position / Freq (Hz)	P 1 Near side		P 2 Upper corner		P 3 Top		P 4 Far side		P 5 Floor	
	Max.	Ave.	Max.	Ave.	Max.	Ave.	Max.	Ave.	Max.	Ave.
1000	8.3	2.8	6.6	1.1	11.1	-3.8	4.6	2.0	2.9	-1.7
1250	5.7	-1.7	5.3	-0.9	4.5	0.2	3.0	-1.2	6.3	-2.9
1600	2.8	0.2	4.6	0.8	6.9	-0.7	5.6	2.4	4.9	1.0
2000	8.3	3.1	7.6	2.6	6.7	-2.3	10.7	4.8	4.2	-1.5
2500	3.5	-1.2	3.9	-0.1	10.4	-3.6	6.6	1.7	7.1	2.9
3150	5.7	1.1	7.3	1.9	6.8	-2.6	6.4	2.6	9.0	3.6
4000	3.6	-1.2	4.7	-0.7	4.8	-1.9	7.1	1.8	4.8	-0.3

4.2 Sound radiated by the rail

Measurements were also carried out on the 1:5 scale model to determine the sound pressure caused by vibration of the rail. A reciprocal approach [35] was followed to infer the sound

pressure distribution on the train external surfaces due to a vibrating rail. According to the principle of vibro-acoustic reciprocity, the transfer function between a point force F acting on a structure at a point A and the resulting sound pressure p at a receiver B is identical to the transfer function between a volume velocity Q of a point monopole located at the point B and the resulting vibration velocity v produced at the original excitation point A. Thus, if a unit force is acting on the rail, the resulting sound pressure on the train external surfaces can be obtained by placing the sound source on the train surfaces and then measuring the vibration velocity of the rail as excited by the sound field. The source orifice was located at various positions along the right-hand upper corner line and on the centreline of the bottom surface and the rail vibration was measured by accelerometers located on the rail, measuring in both vertical and lateral directions, see Figure 17. However, in the present work only the results from the vertical accelerometer are shown.

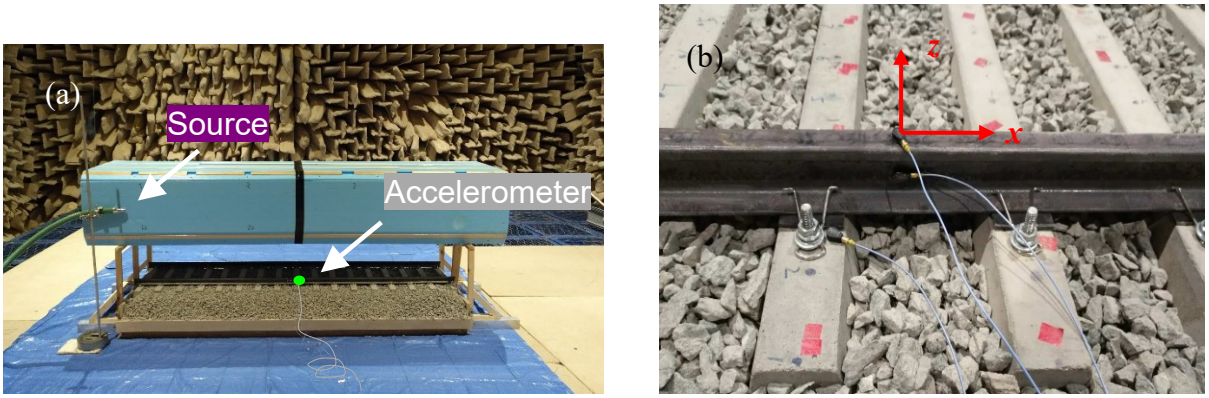

Figure 17. (a) Measurement arrangement for the laboratory test for rail source and (b) the accelerometer locations on the rail.

A numerical model was built with the same geometry as that in the measurement, see Figure 18. The velocity of the rail under a unit force, predicted using the infinite beam model introduced in Section 3.2, and the resulting sleeper vibration were assigned to the boundary elements representing the rail and sleeper in the numerical model. The properties used for the track are listed in Table 3. The velocity of the sleeper was derived using the method given in Section 3.3. The absorption property of the ballast was modelled by using its impedance in the same way as before, but it was only present on the top surface in the region outside the sleepers.

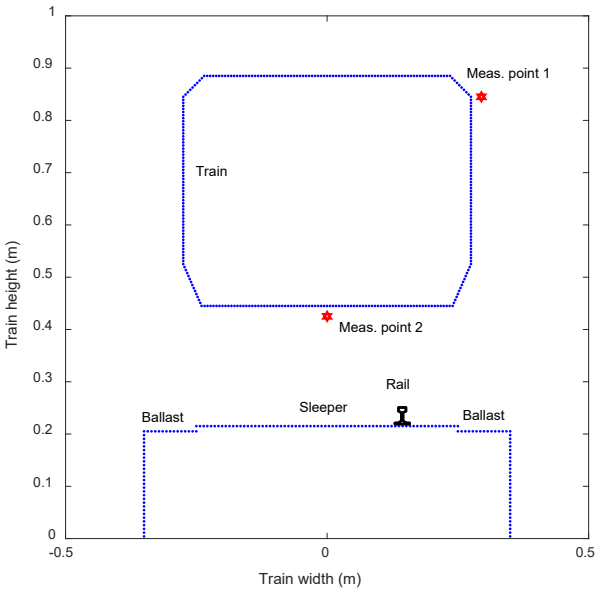

Figure 18. The 2.5D BE model for predicting track noise on train outside surfaces.

Table 3. Parameters used for vertical motion of the 1:5 scale track [31].

Young's modulus	2.1×10^{11} N/m^2
Rail bending stiffness	0.010 MNm^2
Rail mass per unit length	3.4 kg/m
Rail damping loss factor	0.05
Rail density	7850 kg/m^3
Pad stiffness	15 MN/m
Pad damping loss factor	0.2
Sleeper mass (half)	1.41 kg
Sleeper spacing	0.12 m
Ballast stiffness	1.0 MN/m
Ballast damping loss factor	1.0

The comparisons between the predictions and the measurements were made for two positions, P_1 and P_2, as indicated in Figure 18. Based on the principle of reciprocity, the results obtained from the measurement correspond to the ratio of the sound pressure and the force, so they are compared with the predicted sound pressure on the train outside surfaces due to a unit force on the rail. These results are shown in Figure 19 for frequency bands between 1250 and 4000 Hz (between 250 and 800 Hz at full scale). The spatial distribution of the rail vertical vibration is also plotted in the figure, from which it can be seen that the finite length leads to significant

spatial variations that are not captured by the model of the infinite rail but the overall decay with distance is mostly captured.

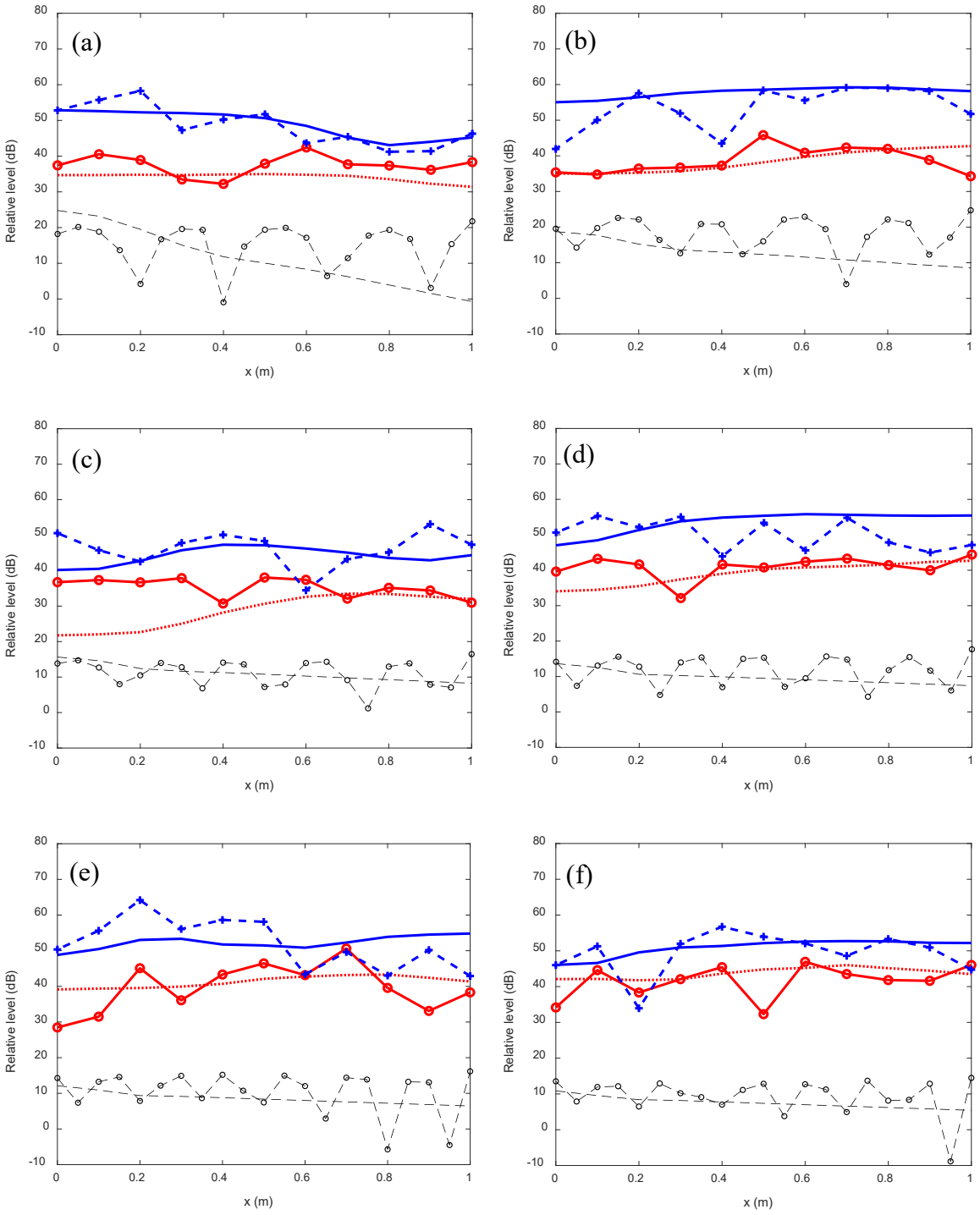

Figure 19. Comparisons between predictions and measurements of the sound pressure level (SPL) on the train external surfaces in one-third octave bands, where x is relative to the force location, dB re 2.0×10^{-5} Pa. ·····: SPL at P1, 2.5D; —o—: SPL at P1, measured; ——: SPL at

P2, 2.5D; - + -: SPL at P2, measured; – – –: rail vibration, predicted; – ⌖ –: rail vibration, measured. (a) 1250 Hz, (b) 1600 Hz, (c) 2000 Hz, (d) 2500 Hz, (e) 3150 Hz, (f) 4000 Hz.

The predictions from the 2.5D model have similar average levels and decay trends to the measurements, although the measured values contain large variations. An important difference between the measurements and the predictions is that the 2.5D approach is based on an infinite rail, whereas in the measurements the rail is finite with a length of only 2 m (10 m at full scale). The wave reflections at the ends of the rail therefore induce spatial variations, as seen from Figure 19.

5 Experimental validation using field measurements

5.1 Measurements on a stationary train

Field measurements [36, 37] were carried out on a metro train in Madrid, Spain, to measure the sound pressure distribution on the train sides when a loudspeaker was located beneath the train floor, see Figure 20. These measurements are used to validate the 2.5D models. The source was located close to a wheel, resting on the ground. The diameter of the source is 0.45 m. Five microphone positions were located on the train side surface directly above the loudspeaker. The height of the first position was 0.1 m above the bottom edge of the sidewall, and the vertical separation between microphone positions was 0.5 m. The result at each microphone position was measured twice.

Figure 20. Measurements of sound pressure on a stationary train. (a) Loudspeaker location, (b) microphone positions, (c) separation of microphones.

To compare with the measured sound pressure levels, a 2.5D BE model was created to predict the sound distribution along the vertical direction on the train sides. The geometry of the train profile in the numerical model corresponds to the train in the tests but the details of the train floor are simplified in the model. The bogie is also omitted. The source in the numerical model has the same size as the loudspeaker and same location relative to the train corresponding to the field test. A half-space ground is considered. Although the source diameter is much larger than the fundamental sources considered in Section 2.3, the response is only considered here in the plane at $x = 0$ so no strong effect is expected. Five field points are set close to the side surface of the train to represent the microphones in the measurements. As the real source strength of the loudspeaker in the field test is not available, the prediction is shifted to correspond to the measured sound pressure levels for ease of comparison. The cross-section of the train and the source and the comparisons of the predicted and the measured sound pressure levels in one-third octave bands (averaged over three frequencies in each one-third band for the prediction) are shown in Figure 21. It can be seen that the sound pressure levels decrease with increasing height on the side surfaces and the predictions match the measurements well.

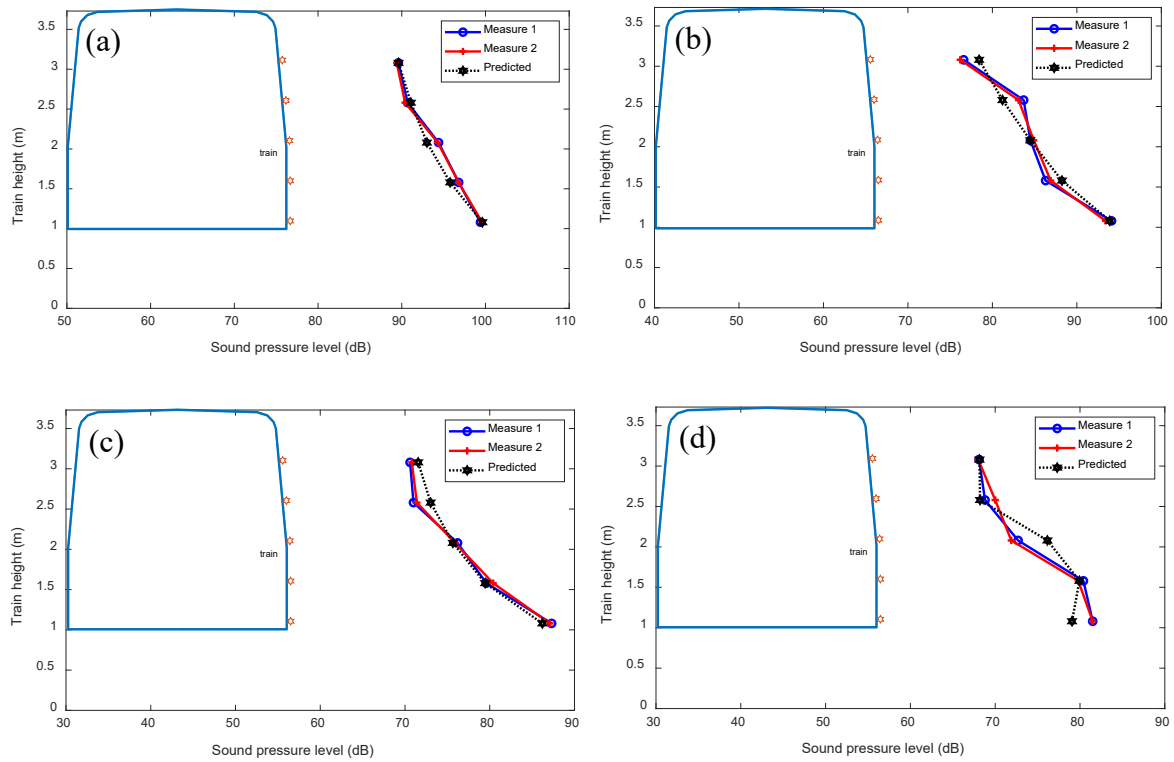

Figure 21. Comparison of prediction and measurement of sound distribution on the train side in one-third octave bands, dB re 2.0×10^{-5} Pa. (a) 200 Hz, (b) 400 Hz, (c) 800 Hz, (d) 1600 Hz.

5.2 Measurements on a running train

The sound pressure distribution was measured on the external surfaces of the metro train when running at 50 km/h on a test track [37]. Four microphones were located on the train side above the bogie area, see Figure 22. They are numbered as points 1006, 1009, 1010 and 1011. Microphones 1006, 1009, 1011 were all 0.7 m above the bottom edge of the sidewall whereas microphone 1010 was 1.5 m above it.

Figure 22. Field measurement positions used to measure sound distribution on the train outside surface.

The numerical models are those given in Figure 12. The sound power of the rail, the wheel and the sleepers were calculated using the TWINS model [7], in which the rail is considered as discretely supported [26]. The parameters adopted in the simulation were based on a field test [37] and are shown in Table 1. Due to uncertainty in the roughness, these predictions have been adjusted to correspond to measured rail and sleeper vibration.

To verify the validity of the prediction of the sound power, three track-side microphones were set to measure the sound pressure levels when the train is passing by, see Figure 23. The sound pressure levels obtained from the predictions and the measurements are compared in Figure 24. Figure 24(a) shows the average of the mean square pressure at the two receivers M1 and M2 and Figure 24(b) shows the result for receiver M3. From these results, it is found that the model can give a good prediction of the rolling noise.

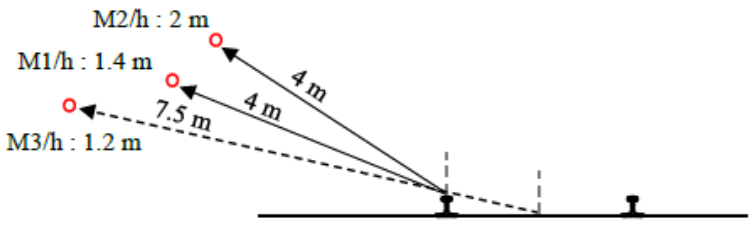

Figure 23. Exterior pressure microphones: M1 and M2 at 4 m from the rail head, M3 at 7.5 m from the centreline of the track.

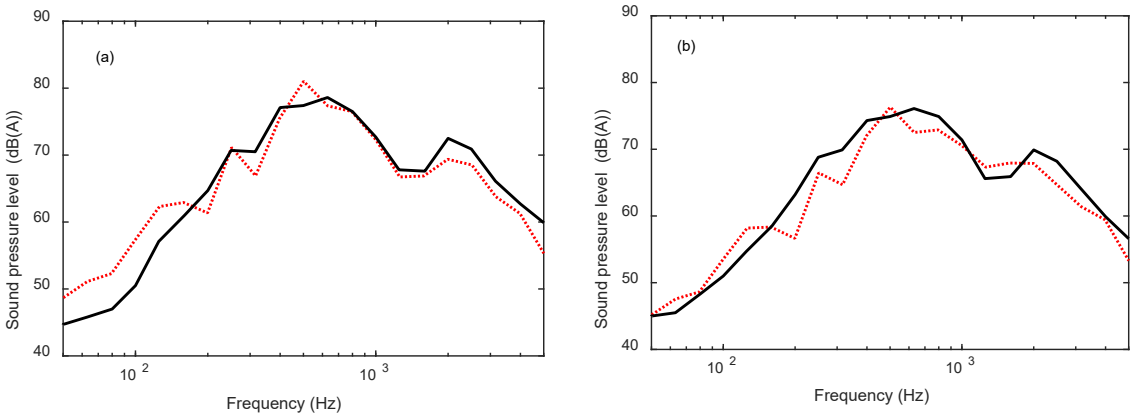

Figure 24. Comparisons between measured and predicted noise levels after correction. (a) Averaged over receivers M1 and M2, (b) receiver M3. —, Measurement; …, TWINS prediction with discrete supports, dB re 2.0×10^{-5} Pa.

The sound power levels from one wheel and from the track vibration associated with one wheel/rail contact calculated from this model are shown in Figure 25. From this, it is clear that the sleepers are dominant at low frequency, the radiation from the wheel radial vibration becomes significant in the 250 Hz band and above 2000 Hz, whereas the rail component, from both vertical and lateral vibration, is dominant in the middle frequency range.

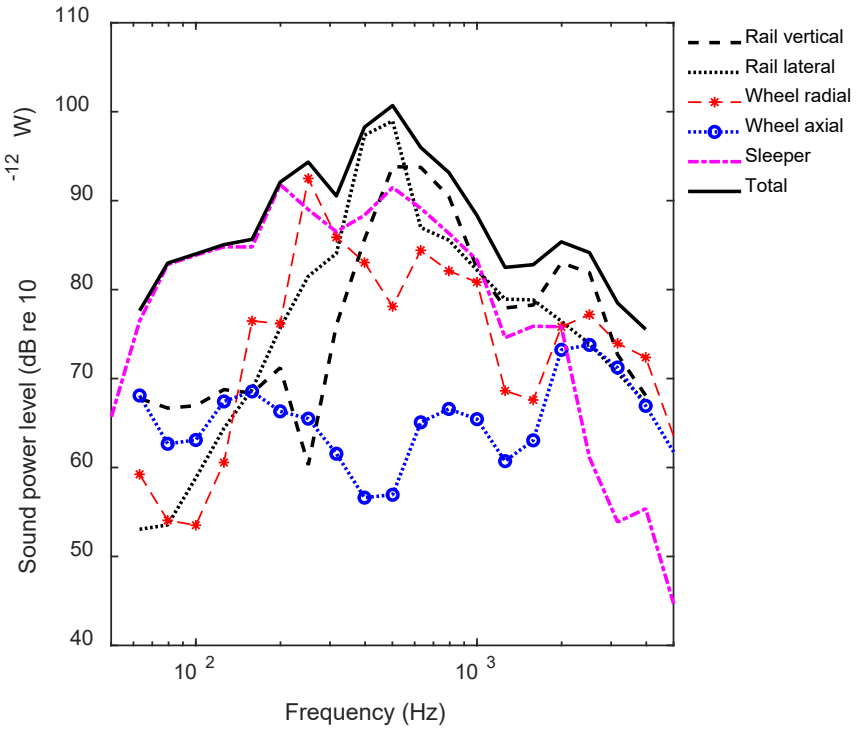

Figure 25. Sound power of the wheel, the rail and the sleepers obtained from TWINS.

These source strengths are then used in the 2.5D predictions of the sound pressure levels at the four positions on the train external surfaces. The total sound pressure on the train surfaces is determined from the incoherent sum of the contributions of the wheel radial and axial components, the rail vertical and lateral components, and the sleepers. Overall A-weighted sound pressure levels on the train external surfaces due to a single bogie (four wheels) are shown in Figure 26. The length of the carriage is 17.92 m and the centre of the bogie is 2.95 m from the carriage end. This sound pressure distribution shows that the highest levels of sound are those incident on the train floor. Moreover, the presence of the fairings helps to create a partially reverberant enclosure below the train. However, noise can also diffract from the edge of the fairings to the side surfaces of the train. The sound level reduces with increasing height. The noise on the train roof due to the wheel and rail is less significant and is estimated to be around 30 dB lower than the noise impinging on the floor.

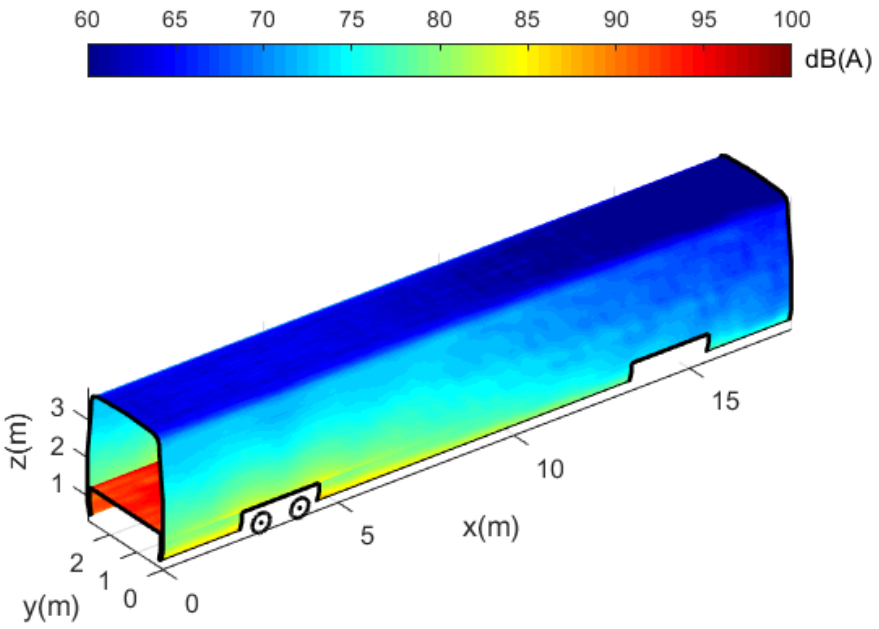

Figure 26. Overall sound pressure levels on the outside surfaces of a single vehicle due to sound sources from a single bogie, dB re 2.0×10^{-5} Pa. The two wheels indiate which bogie is considered.

To compare the prediction with the measurements, the predicted sound pressure levels were calculated by including the contribution from the two bogies below the carriage on which the microphones were mounted and the closest bogie from the adjacent carriage on either side. The comparisons with the measurements are shown in Figure 27 for two positions. The agreement for the other two positions is similar. The predictions capture the main trend of the sound pressure spectra compared with the measurements. However, at low frequency, the predictions are lower than the measurements, whereas they are higher at high frequency. Comparison with Figure 25 indicates that the peak at 500 Hz is dominated by lateral motion of the rail which may be overpredicted due to the neglect of torsion.

The high frequency results may be affected by the simplified consideration of the wheel radiation. The overall sound pressure levels from the predictions and the measurements, together with the relative error between them, are given in Table 4. The relative errors in terms of the overall sound pressure levels are less than 3 dB at these four measurement positions, which shows that the 2.5D model is able to predict satisfactorily the sound pressure on the train external surfaces in running operation.

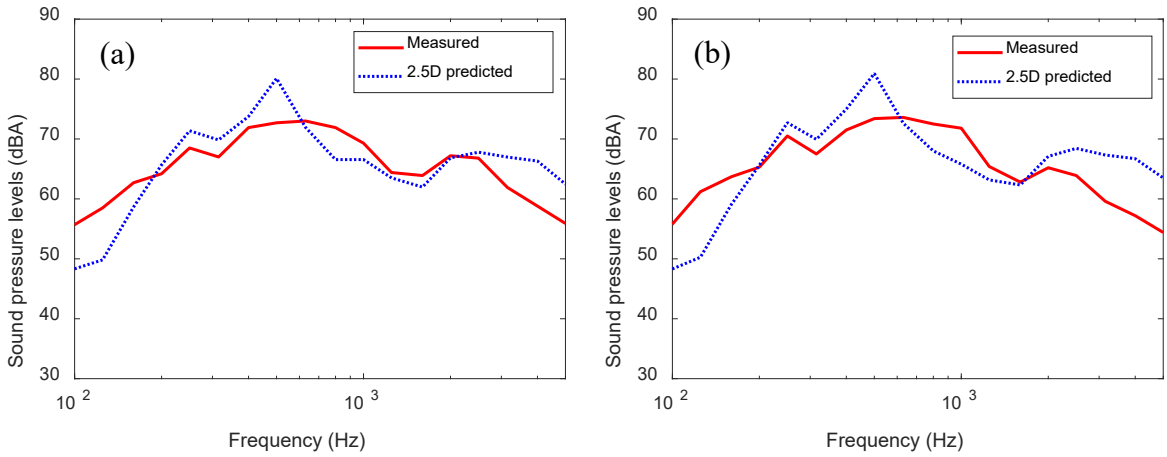

Figure 27. Comparisons between the 2.5D predictions and the measurements on a running vehicle, dB re 2.0×10^{-5} Pa. (a) Point 1006, (b) point 1009.

Table 4. Overall sound pressure levels on the train sides.

	P 1006	P 1009	P 1010	P 1011
Prediction (dB(A))	83.2	83.1	79.7	82.9
Measurement (dB(A))	80.6	81.1	78.3	80.4
Difference (dB(A))	2.6	2.0	1.4	2.5

5.3 Limitations of using the 2.5D method

The experimental validation by the laboratory measurements and the field measurements showed that the 2.5D BE method can be used to predict the sound pressure incident on the train external surfaces due to rolling noise with reasonable agreement. The 2.5D BE model is also much more efficient compared with 3D models. However, the 2.5D method also has some limitations when it is applied to train noise. The wheels are discrete sources, so simplifications had to be made and fundamental sources were used to model them, neglecting their overall size and details of their directivity. As the rail is uniform along its axis, the 2.5D method could be applied to it in a straightforward manner. The finiteness of the train model will also have some effects on the agreement with the laboratory measurements where the scaled train model is relatively short. This is less problematic for the metro vehicle, where the train is longer, but the gaps between two adjacent carriages cannot be included in the model.

In the field measurements, where the metro vehicle was running at 50 km/h, it is reasonable to neglect convective effects caused by the air flow. When the train is running at high speeds,

however, these may be important. These could be included in the 2.5D method by adjusting the acoustic wavenumber to allow for the flow velocity.

A lot of equipment is mounted beneath the train floor, which causes scattering of sound below the vehicle. The 2.5D method is therefore less suitable for predicting the sound pressure incident on the train floor. For wider application, the 2.5D BE method could also be used to predict the exterior noise radiated into the surroundings and even the noise in tunnels.

6 Conclusions

A 2.5D BE approach has been developed to calculate the noise transmission from the wheels, rails and sleepers to the sound pressure on the external surfaces of a train. The wheel was modelled by using approximations to a monopole and a dipole in the 2.5D models. The rail and the sleepers were modelled by their cross-section in the 2D domain and their wavenumber spectrum in the third direction. An inverse Fourier transform was used to convert the sound pressure from the wavenumber domain back to the spatial domain. The TWINS model was used to determine the sound powers of the individual components which were then used to adjust the source level in the 2.5D model predictions. The overall sound pressure level on the train external surfaces was obtained by adding the various components incoherently. Comparisons were made with measurements of sound pressure levels on the external surfaces of a 1:5 scale model train in an anechoic chamber and on a full-scale metro train, both statically and in running operation. The comparisons with the laboratory tests show that the predicted sound pressure levels from the 2.5D model and the measured ones have a similar decay trend along the train axis direction and the average difference of the sound pressure levels is less than 3 dB. For the field measurement on a stationary train, the predicted sound pressure distribution along the train height on the train side is close to that obtained by measurement. In the field measurement on a running train, the predictions and the measurements agree fairly well in terms of sound pressure spectrum and in terms of the overall sound pressure levels the differences are less than 3 dB. The 2.5D BE model can therefore be used to predict the sound pressure on the external surfaces of a train, which is an essential input quantity to evaluate interior noise.

Acknowledgements

The work presented in this paper has received funding from China Scholarship Council and the Shift2Rail Joint Undertaking under the European Union's Horizon 2020 research and innovation programme (grant agreement no. 777564). The contents of this publication only reflect the authors' view and the Joint Undertaking is not responsible for any use that may be made of the information contained in the paper. The authors would also like to thank Dr. Hongseok Jeong for his assistance in the laboratory measurements and Metro de Madrid for assistance in the field tests. The authors are grateful to Dr. Xianying Zhang for providing the measured vibration of the 1:5 scale rail.

References

[1] J. Forssén, S. Tober, A.C. Corakci, A. Frid, W. Kropp, Modelling the interior sound field of a railway vehicle using statistical energy analysis, Applied Acoustics. 73(4) (2012) 307-311.
[2] M. Sadri, J. Brunskog, D. Younesian, Application of a Bayesian algorithm for the Statistical Energy model updating of a railway coach, Applied Acoustics. 112 (2016) 84-107.
[3] P. Shorter, B. Gardner, P. Bremner, A hybrid method for full spectrum noise and vibration prediction, Journal of Computational Acoustics. 11(02) (2003) 323-338.
[4] Z. Tang, Z. Li, Q. Wang, Z.H. Liu, Numerical calculation of the interior noise for the high-speed transportation under coupled multi-physical field excitations, Journal of Vibroengineering. 18(4) (2016) 2641-2655.
[5] H. Jang, C. Hopkins, Prediction of sound transmission in long spaces using ray tracing and experimental Statistical Energy Analysis, Applied Acoustics. 130 (2018) 15-33.
[6] A. Bistagnino, A. Vallespín, J. Sapena, Prediction of Acoustical Wall Pressure Levels of Rolling Stock Vehicles, in Noise and Vibration Mitigation for Rail Transportation Systems. 2015, Springer, 675-682.
[7] D. Thompson, B. Hemsworth, N. Vincent, Experimental validation of the TWINS prediction program for rolling noise, part 1: description of the model and method, Journal of Sound and Vibration. 193(1) (1996) 123-135.
[8] C.M. Nilsson, C.J.C. Jones, D. Thompson, J. Ryue, A waveguide finite element and boundary element approach to calculating the sound radiated by railway and tram rails, Journal of Sound and Vibration. 321(3-5) (2009) 813-836.
[9] X. Zhang, G. Squicciarini, D.J. Thompson, Sound radiation of a railway rail in close proximity to the ground, Journal of Sound and Vibration. 362 (2016) 111-124.
[10] X. Zhang, D.J. Thompson, Q. Li, D. Kostovasilis, M.G. Toward, G. Squicciarini, J. Ryue, A model of a discretely supported railway track based on a 2.5 D finite element approach. Journal of Sound and Vibration. 438 (2019) 153-174.

[11] X. Sheng, T. Zhong, Y. Li, Vibration and sound radiation of slab high-speed railway tracks subject to a moving harmonic load, Journal of Sound and Vibration. 395 (2017) 160-186.
[12] X. Zhang, H. Jeong, D. Thompson, G. Squicciarini, The noise radiated by ballasted and slab tracks, Applied Acoustics. 151 (2019) 193-205.
[13] L. Li, D. Thompson, Y. Xie, Q. Zhu, Y. Luo, Z. Lei, Influence of rail fastener stiffness on railway vehicle interior noise. Applied Acoustics. 145 (2019) 69-81.
[14] P. Geissler, D. Neumann, Modelling extruded profiles for railway coaches using SEA. in Proceedings of the 1999 ASME Design engineering technical conferences, Las Vegas, September. 1999.
[15] G. Xie, D.J. Thompson, C.J.C. Jones, A modelling approach for the vibroacoustic behaviour of aluminium extrusions used in railway vehicles, Journal of Sound and Vibration. 293(3-5) (2006) 921-932.
[16] U. Orrenius, Y.Y. Pang, B. Stegeman, S. Finnveden, Acoustic modeling of extruded profiles for railway cars, in Novem Saint Raphael, 2005.
[17] C.M. Nilsson, A.N. Thite, C.J.C. Jones, D.J. Thompson, Estimation of sound transmission through extruded panels using a coupled waveguide finite element-boundary element method, in Noise and Vibration Mitigation for Rail Transportation Systems. 2008, Springer, 306-312.
[18] Y. Liu, J.C. Catalan, External mean flow influence on sound transmission through finite clamped double-wall sandwich panels, Journal of Sound and Vibration. 405 (2017) 269-286.
[19] Y. Liu, C. Daudin, Analytical modelling of sound transmission through finite clamped double-wall sandwich panels lined with poroelastic materials, Composite Structures. 172 (2017) 359-373.
[20] X. Zheng, Z. Hao, X. Wang, J. Mao, A full-spectrum analysis of high-speed train interior noise under multi-physical-field coupling excitations, Mechanical Systems and Signal Processing. 75 (2016) 525-543.
[21] T. Kohrs, K.R. Kirchner, D. Fast, Sound propagation and distribution around typical tran carbody structures. in InConference Proceedings, Euronoise. 2018.
[22] D. Duhamel, Efficient calculation of the three-dimensional sound pressure field around a noise barrier, Journal of Sound and Vibration. 197(5) (1996) 547-571.
[23] T. Wu, Boundary element acoustics: fundamentals and computer codes. Wit Pr/Computational Mechanics, 2000.
[24] M. Delany, E. Bazley, Acoustical properties of fibrous absorbent materials, Applied Acoustics. 3(2) (1970) 105-116.
[25] F. Fahy, D. Thompson, Fundamentals of sound and vibration, CRC Press, 2016.
[26] D. Thompson, Railway noise and vibration: mechanisms, modelling and means of control, Elsevier, 2008.
[27] T. Kitagawa, D.J. Thompson, The horizontal directivity of noise radiated by a rail and implications for the use of microphone arrays, Journal of Sound and Vibration. 329(2) (2010.) 202-220.
[28] J. Ryue, S. Jang, D.J. Thompson, A wavenumber domain numerical analysis of rail noise including the surface impedance of the ground, Journal of Sound and Vibration. 432(2018).173-191.
[29] J.W. Strutt (Lord Rayleigh), The theory of sound, Dover, 1945.
[30] X. Zhang, D. Thompson, E. Quaranta, G. Squicciarini, An engineering model for the prediction of the sound radiation from a railway track, Journal of Sound and Vibration. 461 (2019) 114921.

[31] X. Zhang, Modelling of track sound radiation, PhD thesis, the University of Southampton, UK, 2016.
[32] H.A. Schenck, Improved integral formulation for acoustic radiation problems, The Journal of the Acoustical Society of America,. 44(1) (1968) 41-58.
[33] L. Ratkevicius, Models of Shielding of Sound Sources on Railway Vehicles. MSc Acoustical Engineering research project, University of Southampton, 2017.
[34] B. Lawrence, Scale model facility for railway vibration and noise. MEng Acoustical Engineering individual project, University of Southampton, 2013.
[35] F.J. Fahy, P. Gardonio, Sound and structural vibration: radiation, transmission and response, Elsevier, 2007.
[36] D. Thompson, X. Liu, H. Li, G. Xie, P. Bouvet, M. Rissmann, L. Baeza, F. Denia, J. Giner, J. Carballeira, J. Martínez, M.L. Trifiletti, Complete virtual test method for structure-borne and airborne noise transmission, RUN2Rail Deliverable 4.2. March 2019 (www.run2rail.eu).
[37] P. Bouvet, M. Rissmann, D. Thompson, X. Liu, H. Li, G. Squicciarini, G. Xie, Validation of complete virtual test method for structure-borne and airborne noise transmission. RUN2Rail Deliverable 4.3, August 2019 (www.run2rail.eu).